UK Atomic Energy Authority

UKAEA-STEP-PR(23)01

Guoliang Xia, Yueqiang Liu, T.C. Hender, K.G. McClements, E. Trier, E. Tholerus

# Control of Resistive Wall Modes in the Spherical Tokamak

# Control of Resistive Wall Modes in the Spherical Tokamak

Guoliang Xia, Yueqiang Liu, T.C. Hender, K.G. McClements, E. Trier, E. Tholerus

This is a preprint of a paper submitted for publication in Nuclear Fusion

# Control of Resistive Wall Modes in the Spherical Tokamak

Guoliang Xia[1], Yueqiang Liu[2], T.C. Hender[1],
K.G. McClements[1], E. Trier[1] and E. Tholerus[1]
[1]UKAEA, Culham Science Centre, Abingdon, OX14 3DB, UK
[2]General Atomics, PO Box 85608, San Diego, CA 92186-5608, USA
E-mail of corresponding author Guoliang.Xia@ukaea.uk

**Abstract**

In this work, the MARS-F/K codes (Liu Y Q *et al* 2000 Phys. Plasmas **7** 3681 & Liu Y Q *et al* 2008 Phys. Plasmas **15** 112503) are utilized to model the passive and active control of the $n$=1 ($n$ is the toroidal mode number) resistive wall mode (RWM) in a spherical tokamak (aspect ratio $A$=1.66). It is found that passive stabilization of the RWM gives a relatively small increase in normalized beta above the no-wall limit, relying on toroidal plasma flow and drift kinetic resonance damping from both thermal and energetic particles. Results of active control show that with the flux-to-voltage control scheme, which is the basic choice, a proportional controller alone does not yield complete stabilization of the mode. Adding a modest derivative action, and assuming an ideal situation without any noise in the closed-loop, the RWM can be fully stabilized with the axial plasma flow at 5% of the Alfven speed. In the presence of sensor signal noise, success rates exceeding 90% are achieved, and generally increase with the proportional feedback gain. On the other hand, the required control coil voltage also increases with feedback gain and with the sensor signal noise.

## 1. Introduction

The Spherical Tokamak for Energy Production (STEP) is a UKAEA program that aims to deliver a prototype compact fusion energy plant and a path to commercial viability of fusion [1]. The low aspect ratio spherical tokamak is attractive because of its potential to achieve high normalized beta $\beta_N = \beta(\%)a(\mathrm{m})B_0(\mathrm{T})/I_p(\mathrm{MA})$ operation (where $\beta$ is the ratio of the volume averaged plasma pressure to the magnetic pressure, and $I_p$ is the total plasma current), since fusion power $\sim \beta_N^2$. To fully exploit this, and to maximize economic attractiveness, operation above the no-wall beta limit is desirable, where the RWM must be controlled either by passive or active control, since otherwise this may lead to a major disruption.

The RWM stability and control have been extensively studied during recent years, because an unstable low-$n$ ($n$ is the toroidal mode number) RWM can limit the operational space of advanced tokamaks, including that designed for ITER [2]. Extensive experimental and theoretical efforts have been devoted to study the RWM stability in conventional tokamaks [3-6], reversed field pinches [7-9], as well as spherical tokamaks [10-13].

The RWM can be viewed as a residual instability from the ideal external kink (XK) mode [14], which in turn is a global magneto-hydrodynamic (MHD) instability driven by plasma current and/or pressure. For a pressure driven XK, the stability is controlled by the normalized beta $\beta_N$. When $\beta_N$ exceeds a critical value (the so-called Troyon no-wall limit [15]), the XK becomes unstable. A close-fitting perfectly conducting wall can stabilize the XK, resulting in increased $\beta_N$. However, by replacing the ideal wall by a resistive wall, the resulting RWM grows on a timescale ($\tau_w$) characteristic of the field penetration time through the wall. An unstable RWM brings the beta limit back to the no-wall Troyon limit. It is thus highly desirable to achieve the RWM stabilization, in order to increase the plasma $\beta_N$ for long pulse or steady state advanced tokamak operations.

It is now well established that either passive control which relies on plasma flow (toroidal and poloidal) and drift kinetic effects [16-18], or active control based on magnetic coils [19-21], or the synergistic actions from both [22, 23], can potentially stabilize the RWM. Within the MHD description, the RWM stabilization mainly comes from the ion sound wave damping and the shear Alfven wave continuum damping [24-27]. The critical toroidal rotation velocity, required for complete stabilization of the mode, is normally a few percent of the Alfven speed [28]. Our recent work shows that poloidal flow (poloidal projection of the parallel flow) can also provide additional stabilization to the RWM [29]. On the other hand, MHD-kinetic hybrid theory, including drift kinetic resonances, predicts substantially lower values (even down to zero) of the critical toroidal rotation speed required for the mode stabilization [30-32]. This model has also shown a cancellation of the drift kinetic damping between the thermal ions and energetic particles (EPs) [33].

Active control of the RWM, using magnetic coils, is feasible thanks to the relatively slow growth of the instability. The basic idea of feedback stabilization of the RWM is to use the magnetic field, produced by current-carrying coils, to actively compensate the field perturbation produced by the mode instability [34-36]. With more realistic control

assumptions, two factors need to be taken into account in the modeling. One is the presence of control sensor noise [37-39]. Another is the control voltage saturation during the feedback control [40, 41]. This issue essentially renders the linear control problem into non-linear control, requiring initial value simulations instead of the typical eigenvalue approach. The latter aspect of voltage saturation is not included in the present work.

The next section introduces a reference spherical tokamak equilibrium. Section 3 reports numerical results of kinetic effects of EPs on the RWM by MARS-K code [16]. Section 4 investigates the feedback control combined with the toroidal rotation on the RWM stability by MARS-F [34]. Section 5 shows numerical results of the feedback control with the sensor noise signal. Section 6 draws conclusion.

## 2. Equilibrium specification and results with fluid model

The equilibrium studied is a case with plasma current $I_p = 21.2$ MA, the major radius $R_0 = 2.5$ m, and $B_0 = 2.8$ T is the toroidal magnetic field at the plasma centre. The case studied has an aspect ratio of $A$=1.66, elongation $\kappa = 2.65$ and triangularity $\delta = 0.4$. The safety factor has values of $q_0 = 2.67$ on the magnetic axis, the minimal value of $q_{\min} = 2.21$ and $q_a = 6.31$ at the plasma edge, the target plasma has the normalized beta value of $\beta_N = 5.04$. Figure 1 shows the radial profiles for some key equilibrium quantities. Normalizations for the plasma pressure, current density and toroidal rotation frequency follow that from reference [42]. The STEP design continues to evolve, and the case studied here represents a particular snapshot during the design process. Since MHD stability depends on non-dimensional parameters, the results are insensitive to the exact device size and studies of RWM stability for a range of STEP cases confirm that the results for the equilibrium considered here are highly representative.

The wall configuration and the assumed set-up for the feedback are shown in Fig. 2. The passive stabilize structure is given by the vacuum vessel and the first wall, though the first wall geometry is simplified by not including the divertor elements. The code MARS-F [34] computed $n$=1 no-wall beta limit as $\beta_N^{no-wall} = 3.59$, and the ideal-wall beta limit as $\beta_N^{ideal-wall} = 5.58$ (the $n$=2 modes are more stable than the $n$=1). Each of the physics models of the MARS-F/K codes (the single fluid mode with plasma flow model [3, 24, 29], the MHD-kinetic hybrid formulation [16], magnetic feedback [34]), that are

relevant to the RWM and that we shall employ in this study, have previously been reported in separate publications, and for brevity are not repeated here. In our calculations, we choose the pressure scaling factor $C_\beta = (\beta_N - \beta_N^{no-wall})/(\beta_N^{ideal-wall} - \beta_N^{no-wall}) = 0.73$ for the target plasma, which shown in Fig. 3, for the RWM study. Assuming a set of active coils located near the outboard mid-plane of the torus, the active coil spans ±18.9 degrees, along with a coincident sensor coil measuring the poloidal field perturbation for the feedback control.

Figure 4 shows the marginal wall position versus the normalized beta. The stability window decreases with increasing $\beta_N$, and the RWM becomes unstable when $\beta_N > 4.35$. The vertical dash-dotted line indicates the no-wall beta limit, and the ideal-wall limit at *d/a*=1.12 is consistent with that computed in Fig. 3. Note in the simulations of the RWM, a plasma rotation is considered $\Omega_0 = 0.05\ \Omega_A$; the XK calculations assume no plasma flow and an ideal wall at normalized position *d/a*. The effect of plasma flow on the RWM is reported in Fig. 5, showing that plasma flow is not a strong influence on the reported results. In particular for the target plasma, the plasma flow cannot stabilize the RWM, motivating inclusion of the kinetic effects on the RWM stability (next section).

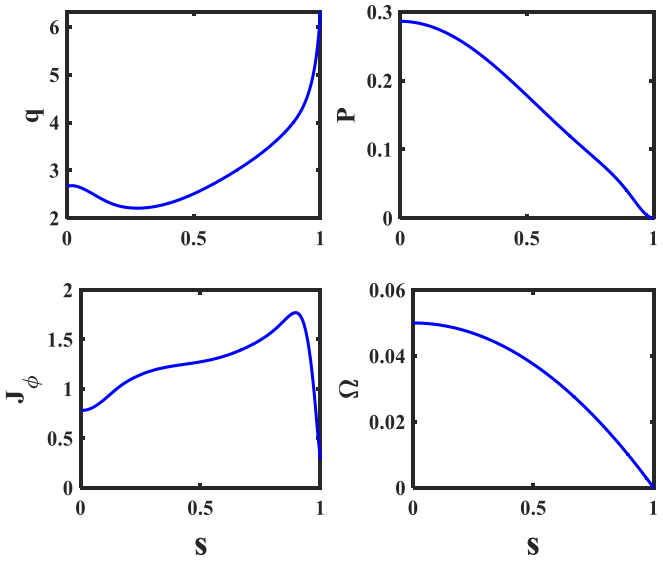


**Figure 1.** The safety factor, plasma pressure, toroidal current and toroidal flow profiles versus the magnetic surface label *s* (the square root of the normalized poloidal flux). The toroidal rotation is not self-consistently included in the equilibrium, and is parameterized by its central value, $\Omega_0$.

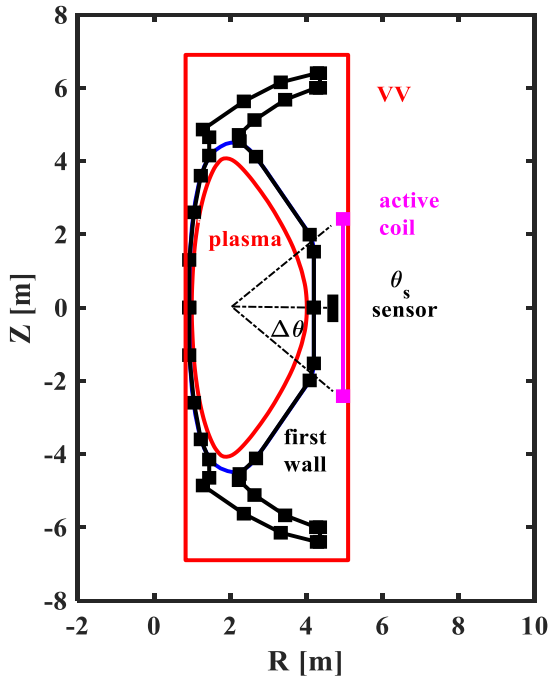


**Figure 2.** Geometry of the RWM stabilization scheme: the RWM passive stability is given by the double wall structure of the assumed simple vacuum vessel (rectangular square in red) and the first wall (in black). The first wall geometry is simplified (blue line) by not including the divertor elements. A midplane active feedback coil (in pink) is assumed along with a coincident sensor coil measuring the poloidal field perturbation. The active coil spans ±18.9 degrees.

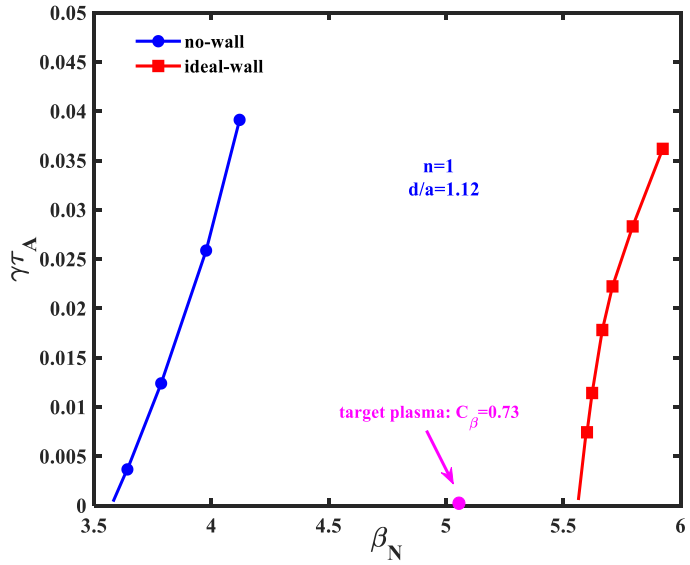


**Figure 3.** The ideal growth rates of the $n$=1 XK with no-wall (circles) and ideal-wall (squares) versus the normalized beta. The position (the first wall) of the ideal-wall is at $d/a$=1.12.

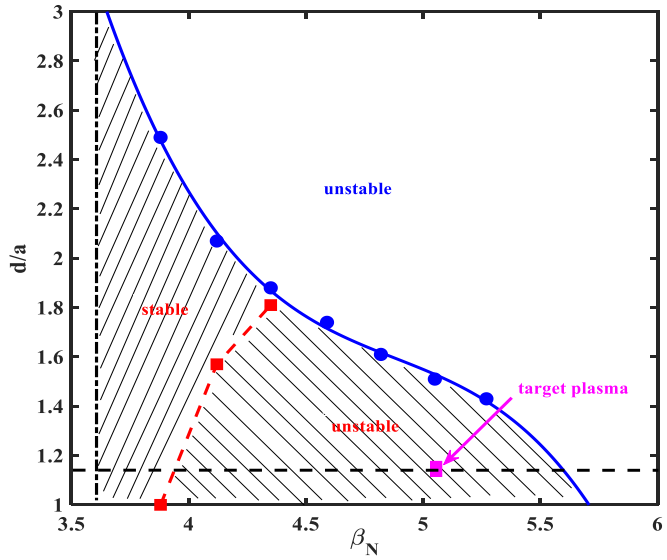


**Figure 4.** The marginal wall position versus normalized beta for the RWM (squares) and XK (circles). The RWM becomes unstable when $\beta_N > 4.35$. The vertical dash-dotted line indicates the no-wall beta limit $\beta_N^{no-wall} = 3.59$; the horizontal dashed line indicates the position of first wall at *d/a*=1.12. In the simulations of the RWM, a plasma rotation is considered $\Omega_0 = 0.05\ \Omega_A$; the XK stability is computed assuming an ideal-wall without plasma rotation. The regions identified as stable and unstable are with respect to the RWM.

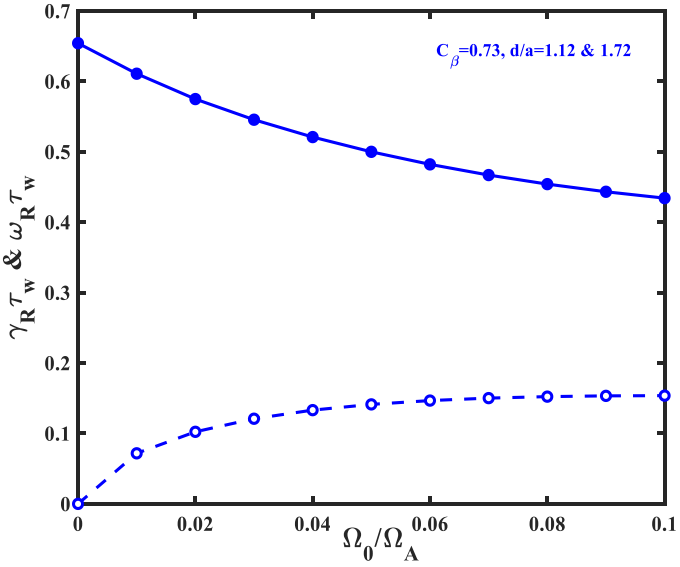


**Figure 5.** The computed eigenvalue (normalized to the wall time, $\tau_w = 10^5 \tau_A$) of the $n$ = 1 RWM versus the on-axis plasma flow, with the target plasma $C_\beta = 0.73$ and the position of the double wall at *d/a*=1.12 and 1.72. The closed symbols indicate the growth rate and the open symbols the mode frequency.

## 3. Kinetic effects on the RWM stability

In this work, we consider drift kinetic effects of both thermal and energetic particles on the RWM stability. We will model the EPs due to Neutral Beam Injection (NBI), which is a possible heating/current drive scheme for tokamaks. A consideration is whether the EPs from the NBI have any significant effect on the RWM stability. The assumed NBI parameters are as follows: two deuterium beams are injected, with a 3.0 m tangency radius for an on-axis beam and a 3.5 m tangency radius for an off-axis beam, with both beamlines being horizontal (i.e. not tilted to match the field line pitch). For the on-axis beam the injection energy is 1 MeV, and the power ($P_{NBI}$) is 11 MW. For the off-axis beam, the injection energy is 500 keV, with $P_{NBI}$ = 71 MW. With these NBI parameters, the fast particle normalized distribution function (density and pressure) is calculated using the ASCOT code [43] as show in Fig. 6.

The particular analytic model for the pitch angle distribution in the MARS-K code [16, 44] assumes a symmetric trapped particle distribution, whereas the numerically computed distribution by ASCOT is not perfectly symmetric due to minor radius averaging and finite orbit effects (Fig. 7). However, this small discrepancy is not thought to be important in terms of the effect on the RWM stability.

Various resonances between the plasma $\mathbf{E}\times\mathbf{B}$ frequency ( $\omega_E$ ) – effectively representing the mode frequency in the plasma frame, and plasma particle drift frequencies (for both thermal and energetic particles), represent opportunities for the continuum spectra damping (the Alfven continuum and/or the ion acoustic damping), as well as kinetic damping of the RWM. These frequencies are compared in Fig. 8, where the particle drift frequencies are averaged values over the particle velocity space.

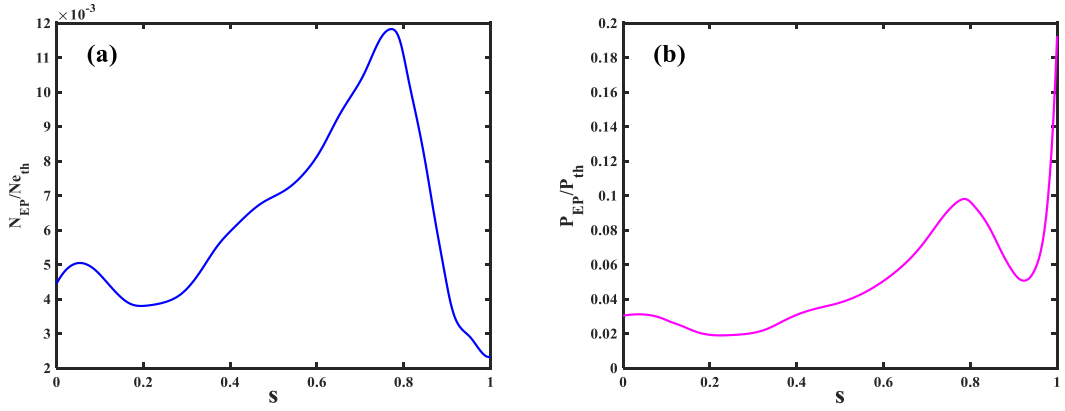


**Figure 6.** The radial profiles of (a) the density and (b) the equilibrium pressure fraction for the EPs obtained by the ASCOT simulation for the equilibrium studied.

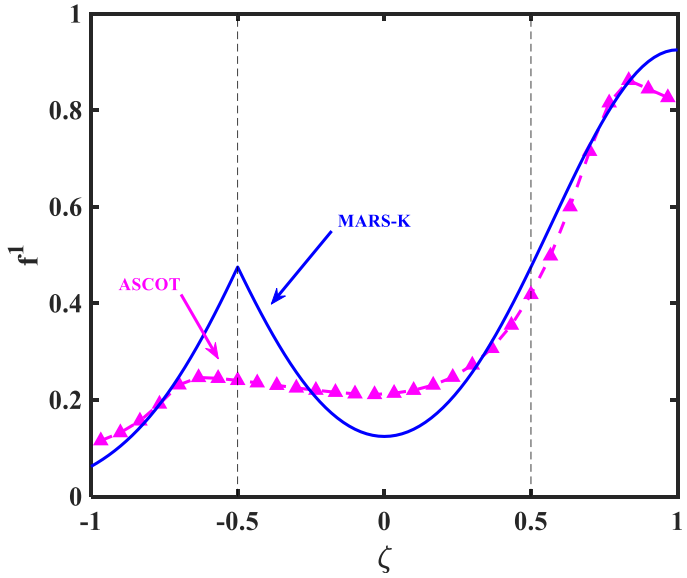


**Figure 7.** Comparison of the pitch angle distribution between ASCOT (pink curve) and the MARS-K (blue curve) model fit for the EPs. In the anisotropic NBI beam model (Gaussian distributions in particle pitch angle space), with the parameters Gaussian centre $\zeta_0 = 0.87$ and width $\delta\zeta_0 = 0.58$ for particles located at the minor radius of $s$=0.5.

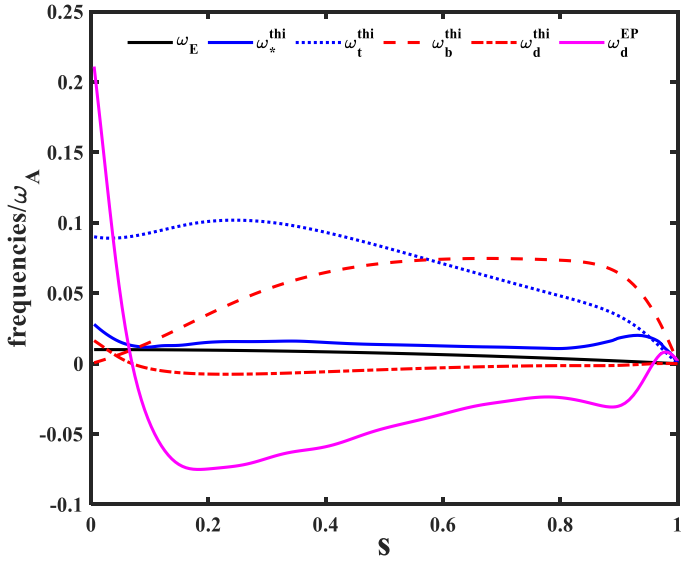


**Figure 8.** Comparison of various frequencies participating in mode-particle Landau resonances: $\omega_E$ is the $\mathbf{E}\times\mathbf{B}$ drift frequency, $\omega_*$ the diamagnetic drift frequency, $\omega_t$ the transit frequency, $\omega_b$ the bounce frequency and $\omega_d$ the precession drift frequency. The precession, bounce and transit frequencies are averaged in the particle velocity space as well as along the poloidal angle of the magnetic flux surface. Here a superscript "*thi*" indicates thermal ions and "*EP*" for fast ions.

Calculations with MARS-K for the $n$=1 RWM show a very weak effect on the growth rate from the NBI ions (Fig. 9). Here $\alpha_D$ is the degree to which the fast ion contribution is included: $\alpha_D$ =0 means no drift kinetic effect (recovers the fluid limit) and $\alpha_D$ =1 corresponds to the physical MHD-kinetic hybrid result. Note that only the precessional drift resonances of trapped thermal and energetic particles are considered in Fig. 9. This is because other types of drift frequencies (transit and bounce) are too high (Fig. 8) compared to the mode frequency (in the plasma frame) to produce significant resonances [44].

The resonance strength varies with the plasma toroidal rotation from the NBI momentum. For a realistic range of toroidal rotation velocities (central frequency, $\Omega_0$, up to 10% of the toroidal Alfven frequency), there is a limited effect of both thermal and energetic particles on the RWM growth rate (Fig. 10). Note that the EPs contribution slightly destabilizes the RWM. This happens when the imaginary part of the perturbed potential energy due to drift kinetic contributions from thermal and energetic particle partially cancel each other [33]. The imaginary part of the perturbed potential energy is always stabilizing for the RWM. Although the effects of alpha particles on the RWM has not been considered for the presented equilibrium, studies for another case show these, like the NBI effects, are weak.

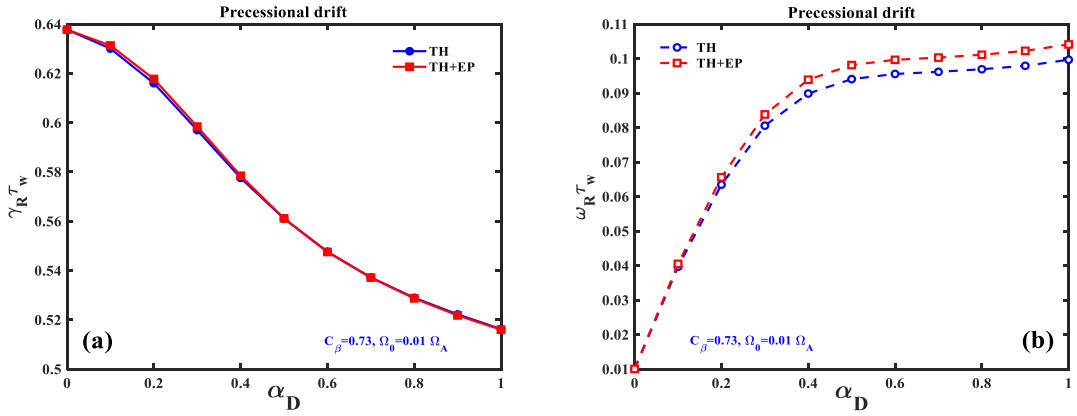


**Figure 9.** (a) Growth rate and (b) mode frequency (normalized to the wall time, $\tau_w = 10^5 \tau_A$) of the MARS-K computed $n$=1 RWM versus the drift kinetic fraction parameter $\alpha_D$. Compared are two cases with or without inclusion of the EPs (due to NBI). The plasma pressure corresponds to $C_\beta = 0.73$ and the on-axis plasma rotation is $\Omega_0 = 0.01\,\Omega_A$.

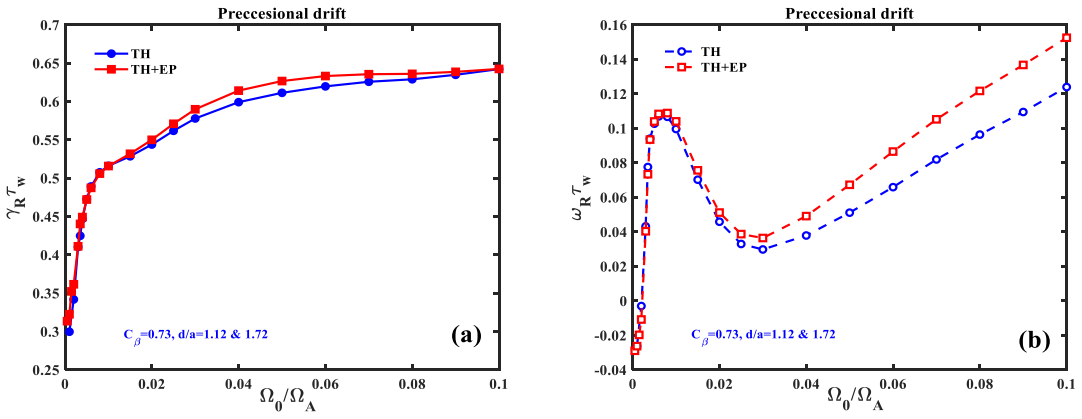


**Figure 10.** (a) Growth rate and (b) mode frequency versus the toroidal rotation $\Omega_0$ at plasma centre. Simulated with preccesional drift resonance alone and compared are two cases with or without inclusion of the EPs. The plasma pressure corresponds to $C_\beta = 0.73$ and the position of the double wall is at *d/a*=1.12 and 1.72.

## 4. Synergetic effects of feedback control and plasma flow on the RWM stability

In this work, the MARS-F code [34] is utilized to model feedback schemes for controlling the *n*=1 RWM in STEP. Before looking at the effects of noise on the RWM feedback, it is necessary to establish the parameters for successful control in the absence of noise. The feedback equation for the active coils, representing the control logic, is written as

$$\frac{d\psi_f}{dt} + R_f I_f = V_f = -G\left(K_p + K_d \tau_f \frac{d}{dt}\right) b_s \qquad (1)$$

where $\psi_f$ is the perturbed magnetic flux through the active coils, $I_f$ the coil current, $R_f$ the resistance of the active coils, $V_f$ the control voltage, and $\tau_f$ the L/R response time of the active coils. $b_s$ is the sensor signal, defined as the poloidal magnetic field perturbation at the low-field side outboard mid-plane at the sensor location (Fig. 2). $K_p$ and $K_d$ are dimensionless feedback gain factors, introduced to effectively simulate an ideal proportional-derivative (PD) controller, and $G$ is the (complex) feedback gain. Equation (1) represents the so-called flux-to-voltage control scheme. It should be noted with the flux-to-voltage control logic, even in the absence of feedback control ($V_f = 0$), the active coils do provide a weak passive stabilizing effect of ~10% on the RWM growth rate as shown in Fig. 11. The same control logic has been assumed in previous RWM control studies for ITER [38, 45]. This is a reasonable choice of the control scheme, since (i) the current in the active coils is eventually driven by the power supply voltage even in

the so-called flux-to-current control scheme, and (ii) the flux-to-current scheme does not allow flexibility in the case of current saturation, i.e. as soon as the current limit is reached, the RWM control is lost [40].

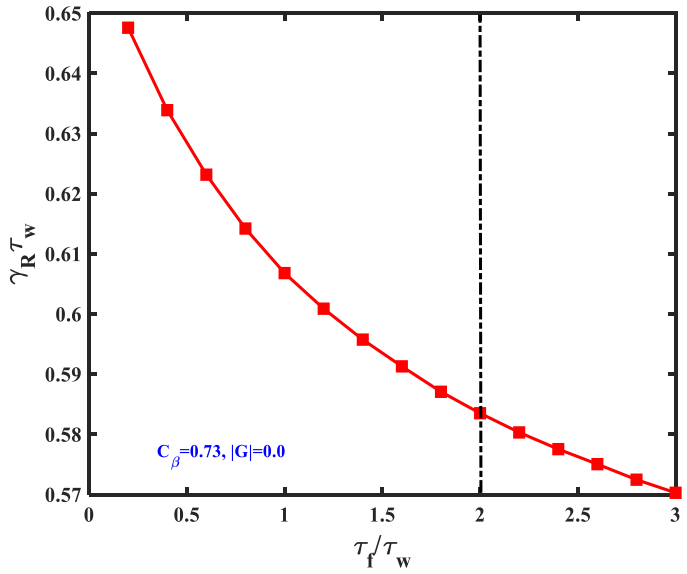


**Figure 11.** The MARS-F computed open-loop growth rate of the $n$=1 RWM versus the ratio of the response time $\tau_f$ of the active coils to the resistive wall time $\tau_w$. The plasma pressure corresponds to $C_\beta = 0.73$ and without plasma flow. The chosen default value for this study is $\tau_f / \tau_w = 2$ (the dash-dotted vertical line).

The simulations above revealed that the passive approach cannot fully suppress the RWM for the case studied, and thus that feedback control is necessary in order to operate above the no-wall limit. Figure 12 shows that with a purely proportional (P) controller, it has proven difficult to attain full feedback stabilization, even with high gains. Note that the abrupt change of the eigenvalue behavior at certain feedback gain value (e.g. at $|G|$~3.2 with $C_\beta = 0.73$) is due to the merging of two branches of closed-loop solutions into a complex conjugate pair, resulting in a RWM instability that weakly depends on the feedback gain. The other less unstable branch, before the root-merging occurs, is not shown in Fig. 12. This root-merging process sometimes happens in the RWM feedback modelling, and appears to be robust against variation of the plasma conditions, such as plasma toroidal flow, kinetic effects in Fig. 13, and coil systems (e.g. the poloidal location of the sensor coils) in spherical tokamak modelling. Even with a fairly large reduction in normalized beta, such that $C_\beta = 0.51$, marginal stability is just achieved in both

eigenvalue and initial value calculations. The root-merging has been observed in conventional tokamaks [41], but could be resolved there by altering the sensor location, in contrast to the spherical tokamak results presented here.

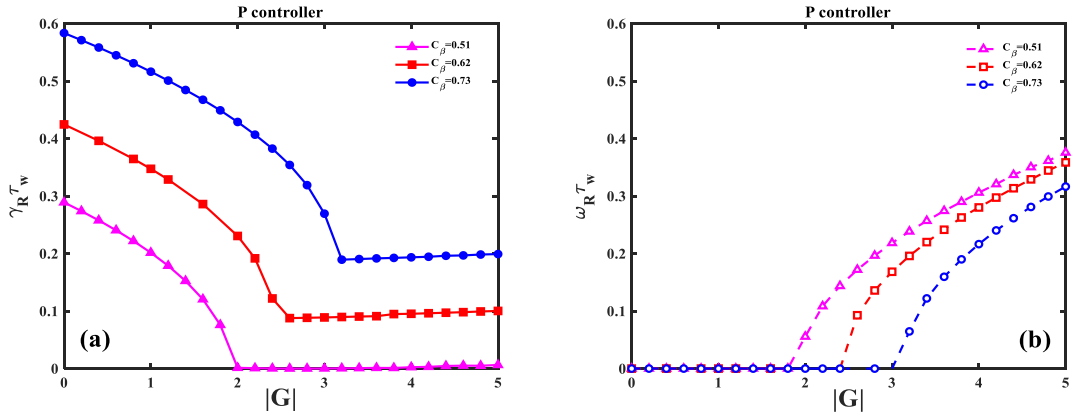


**Figure 12.** (a) Growth rate and (b) mode frequency of the MARS-F computed $n$=1 RWM versus the feedback gain amplitude for various values of $C_\beta$, simulated with a P controller $K_p$=1, $K_d$=0 and without plasma flow.

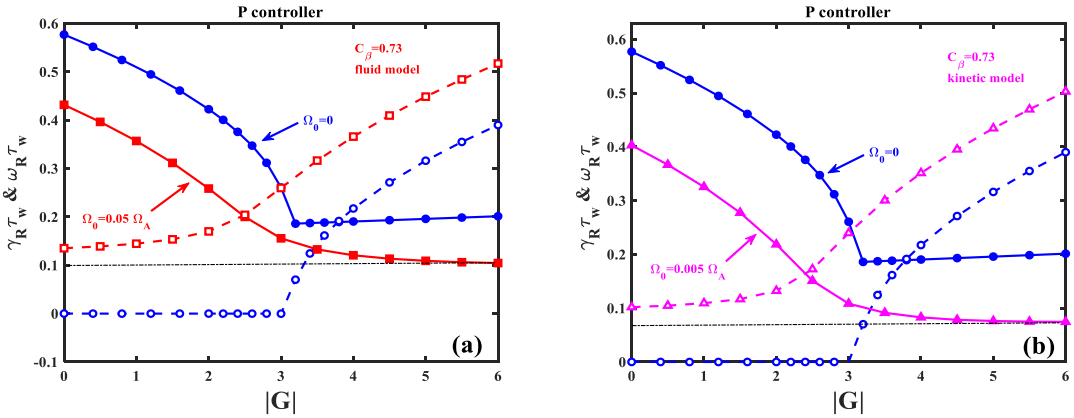


**Figure 13.** The computed closed-loop eigenvalue of the $n$=1 RWM, assuming (a) fluid model and (b) kinetic model combined with the plasma flow. The kinetic model includes preccesional drift resonance. The plasma pressure corresponds to $C_\beta = 0.73$, the plasma flow in the fluid model is $\Omega_0 = 0.05\ \Omega_A$ while in the kinetic model this value is $\Omega_0 = 0.005\ \Omega_A$. The solid curves indicate the growth rate and the dashed curves the mode frequency.

As a result, a weakly unstable residual (and rotating) closed-loop RWM remains with a P only controller, even at large feedback gain. The difficulties in achieving feedback stabilization with a solely P controller motivates exploring a PD controller. Including

toroidal plasma rotation at $\Omega_0 = 0.05\ \Omega_A$ allows feedback stabilization with a relatively small derivative term ($K_d$ =0.3) as shown in Fig. 14. The results in Fig. 15 show that the critical feedback gain value for fully suppressed the mode decrease with $C_\beta$, and this value also decreases with increasing the derivative gain factor $K_d$ as shown in Fig. 16. The disadvantage of high derivative gain is that it accentuates the effect of noise on the sensor signal, as discussed in the next section.

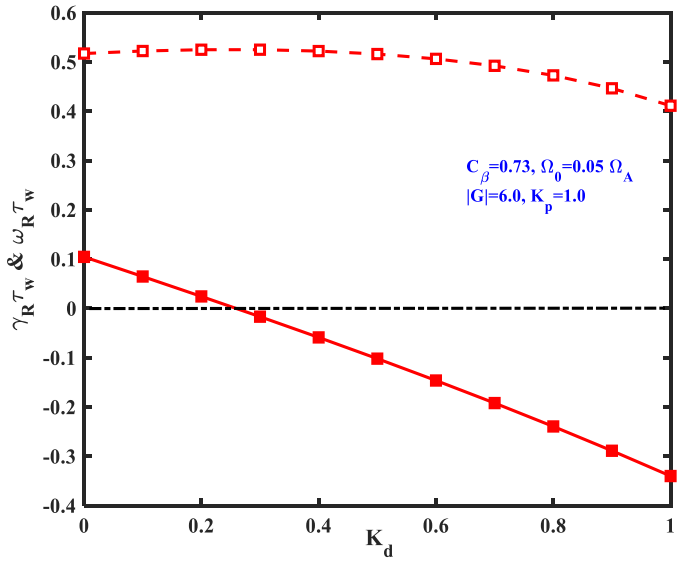


**Figure 14.** The MARS-F computed eigenvalue of the $n$ = 1 RWM versus the derivative gain factor. The plasma pressure corresponds to $C_\beta = 0.73$, the on-axis plasma rotation is $\Omega_0 = 0.05\ \Omega_A$ and the feedback gain amplitude $|G| = 6$. The closed symbols indicate the growth rate and the open symbols the mode frequency.

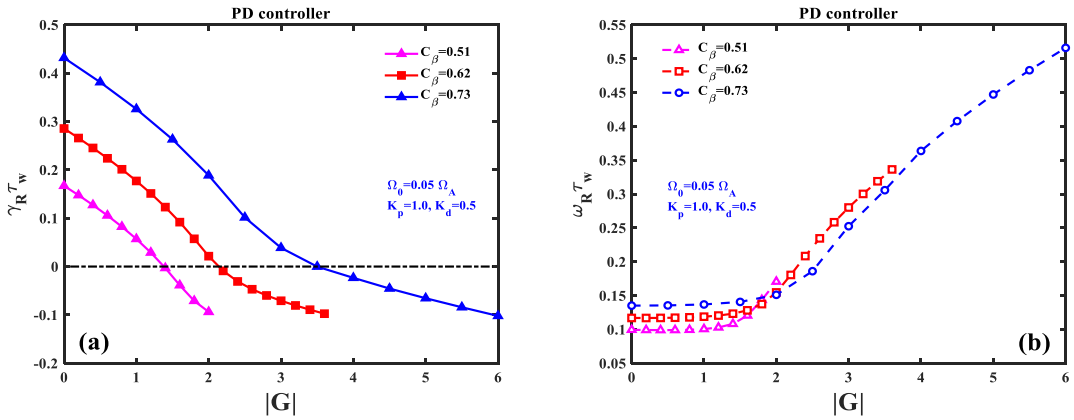


**Figure 15.** (a) Growth rate and (b) mode frequency of the computed $n$ = 1 RWM versus the feedback gain amplitude for various values of $C_\beta$, simulated with a PD controller $K_p$=1.0, $K_d$=0.5 and the on-axis plasma rotation is $\Omega_0 = 0.05\ \Omega_A$.

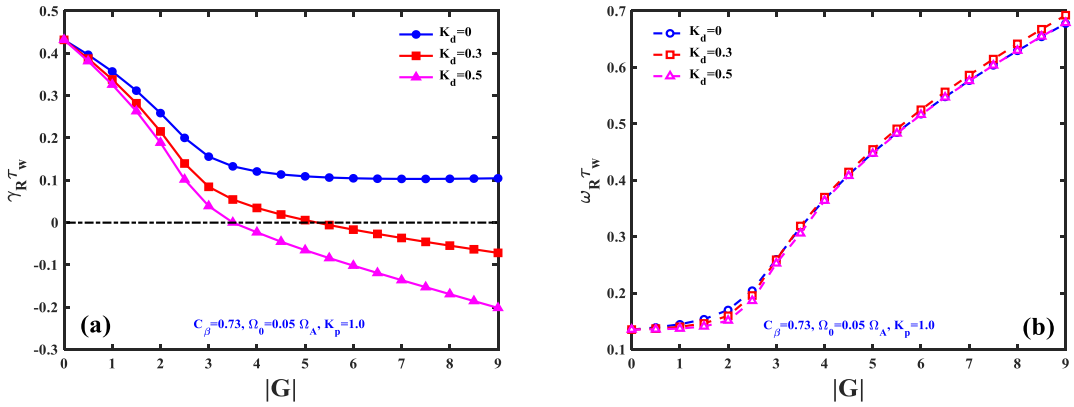


**Figure 16.** (a) Growth rate and (b) mode frequency of the computed $n$ = 1 RWM versus the feedback gain amplitude, for various values of derivative gain factor $K_d$. The plasma pressure corresponds to $C_\beta = 0.73$ and the on-axis plasma rotation is $\Omega_0 = 0.05\ \Omega_A$.

## 5. Effect of the sensor signal noise on the RWM stability

A key aspect in the performance of feedback controller is the presence of noise in the detected signal(s). The sensor signal $b_s$ is replaced by $b_s = b_s^0 + b_s^{noise}$, when the white noise is taken into consideration. The control calculations are dependent on the system noise, and this issue has been studied by Liu [37]. In this study, high-frequency noise measured by magnetic sensors, at levels above the typical frequency of resistive wall modes, was analyzed across a range of tokamak devices including DIII-D, JET, MAST, ASDEX Upgrade, JT-60U, and NSTX. A high-pass filter enabled identification of the noise component with Gaussian-like statistics that shares certain common characteristics in all devices considered. A conservative prediction was made for the high-frequency noise component of the sensor signals, to be used for resistive wall mode feedback stabilization, based on the multimachine database. The predicted root-mean-square $n$ = 1 noise level is $10^1$ to $10^5$ G/s for the voltage signal (time derivative of the perturbed magnetic field), and $10^{-4}$ to 1 G for the perturbed magnetic field itself (so there is considerable spread in the data).

Initial value simulations show without sensor noise that stabilization is rather marginal at $K_d$ =0.3. However increasing to $K_d$ =0.5 gives clear stabilization (Fig. 16), which at high gains can strongly stabilize the RWM. Figure 17 shows the simulated time traces (a) the poloidal sensor signal, (b) the current, and (c) the voltage for various feedback gain amplitude with PD controller. Note these $|G|$ values are larger than the critical gain computed with eigenvalue approach, ensuring closed-loop stability as the derivative

action tends to amplify the sensor noise. In the absence of sensor noise, Fig. 17(a) shows the sensor signal is damping more quickly with higher feedback gain value, and the damping frequency (mode frequency) is the same as simulated in Fig. 16(b). The feedback control is switched on at 65.7 ms, when the perturbed magnetic field is $|b_s|$=1.25 G. The high feedback gain means high power needed in the active coils, e.g. in Fig. 17(c) the required voltage of $|G|$=20 is double of that for $|G|$=10.

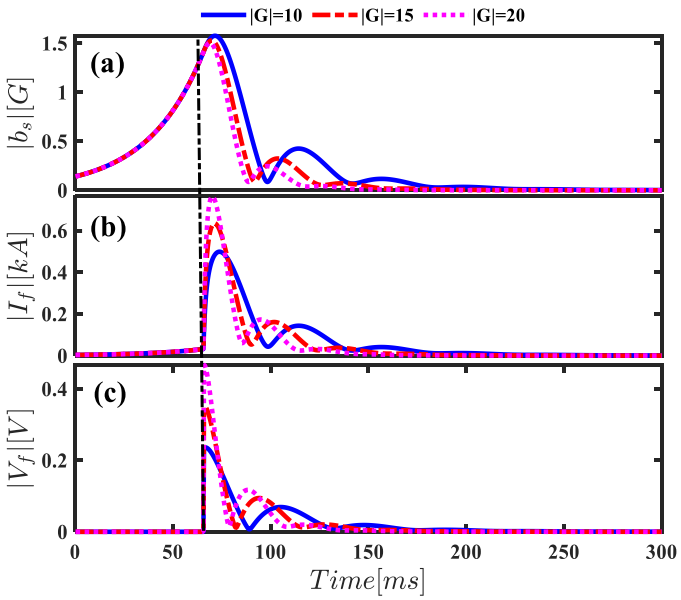


**Figure 17.** Initial value simulation of the $n$ = 1 RWM control for various values of the feedback gain amplitude with a PD controller $K_p$=1.0, $K_d$=0.5, in the absence of sensor noise. Plotted are the time traces of (a) the amplitude of the poloidal sensor signal, (b) the current amplitude in the active coils, and (c) the voltage of the active coil power supply. The feedback is activated at 65.7 ms (vertical dash-dotted line). The plasma pressure corresponds to $C_\beta = 0.73$ and the on-axis plasma rotation is $\Omega_0 = 0.05\ \Omega_A$.

With more realistic control assumptions, i.e. the presence of sensor signal noise, the RWM feedback is found to be of a more subtle issue for the equilibrium studied. This is partially due to the fact that the derivative action tends to amplify the sensor noise, and partially related to the statistic nature of the problem leading to difficulties e.g. in judging the success of mode suppression in certain cases. In the present study, random numbers with normal distribution, zero mean and standard deviation of $\sigma_{noise} < 1$ G, are injected into the perturbed magnetic field sensor signal, when the closed-loop system is modelled

with the initial value approach. Compared with Fig. 17, a sensor noise $\sigma_{noise} = 0.1$ G is included in the closed-loop calculations as shown in Fig. 18(d), the required power supply of the voltage and current significantly increases. The horizontal dash-dotted lines in Fig. 18(c) indicate the maximum required voltage.

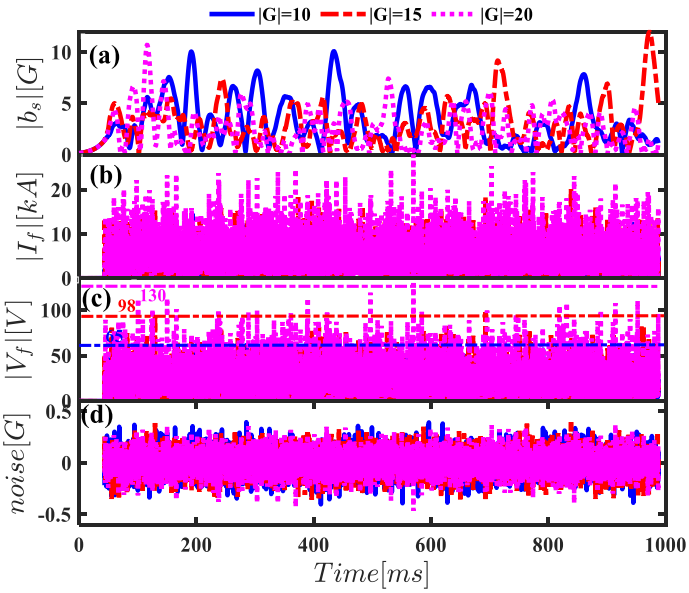


**Figure 18.** Initial value simulation of the $n$ = 1 RWM control for various values of the feedback gain amplitude with sensor noise. Plotted are the time traces of (a) the amplitude of the poloidal sensor signal, (b) the current amplitude in the active coils, (c) the voltage of the active coil power supply and (d) machine-generated noise sequence with Gaussian distribution and standard deviation of $\sigma_{noise} = 0.1$ G . The plasma pressure corresponds to $C_\beta = 0.73$ and the on-axis plasma rotation is $\Omega_0 = 0.05\ \Omega_A$. The horizontal dash-dotted lines in (c) indicate the maximum required voltage.

This control with the PD controller can be tolerant to a realistic noise level of ~0.1 G in the detection system, but not all cases are successfully stabilized, such as the case of $|G|$=15 is unstable in Fig. 18. With noise the question of whether the feedback scheme is successful becomes a statistical issue of running many simulations. A criterion, based on the total perturbed magnetic energy of the system as shown in Fig. 19, is proposed to judge the control loop success. The perturbed energy of $|G|$=10 and $|G|$=20 decreases with the simulation time, i.e. the RWM becomes stable. While the perturbed energy of $|G|$=15 increases as well as the sensor signal in Fig. 18(a). To obtain reliable results, 100 initial value closed-loop simulations are performed for the same feedback configuration,

with statistics drawn in terms of the success rate for the RWM suppression. In Fig. 20, we report the simulated success rate versus the feedback gain amplitude. It is found that success rates exceeding 90% are achieved, and generally increase with the proportional feedback gain and the required control coil voltage also increases with feedback gain. On the other hand, the success rates decrease with increasing the sensor signal noise as shown in Fig. 21. The required control coil voltage increases with the sensor signal noise.

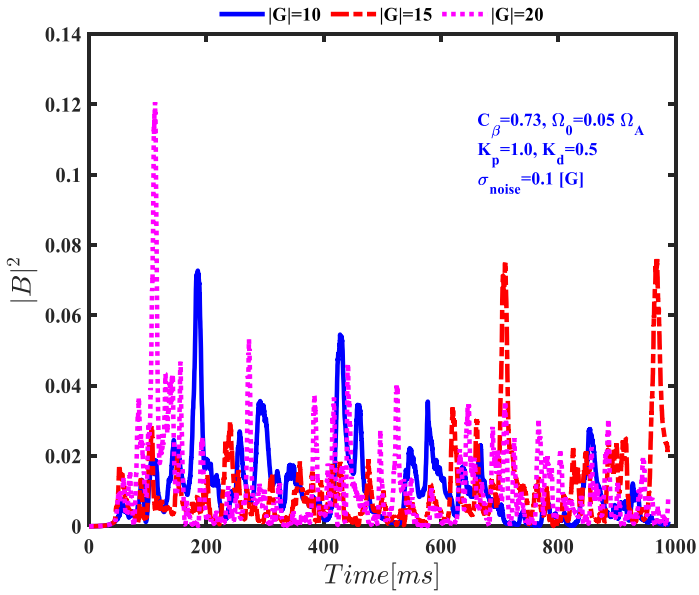


**Figure 19.** Simulated time traces of the total perturbed magnetic energy of the plasma-coil system for various values of the feedback gain amplitude. Simulated with a PD controller $K_p$=1.0, $K_d$=0.5, the sensor noise has standard deviation of $\sigma_{noise} = 0.1$ G, the plasma pressure corresponds to $C_\beta = 0.73$ and the on-axis plasma rotation is $\Omega_0 = 0.05\ \Omega_A$.

The alternative way is via assessing whether the control is sufficient to avoid disruption. Reference [46] predicts the amplitude of $n$=1 locked modes to trigger a disruption. The result is

$$B_{ML} = c * q_{95}^{a_q} * li(3)^{a_{li}} * \rho_c^{a_\rho} * B_\theta \qquad (2)$$

where $q_{95}$ is the safety factor at $s$=0.95, the internal inductance $li(3) = 2V\left\langle B_\theta^2 \right\rangle / \mu_0^2 I_p^2 R_0$, $B_\theta$ the poloidal magnetic field, $\mu_0$ the vacuum magnetic permeability, the plasma volume $V$ and the normalized distance from the magnetic centre of the plasma to the

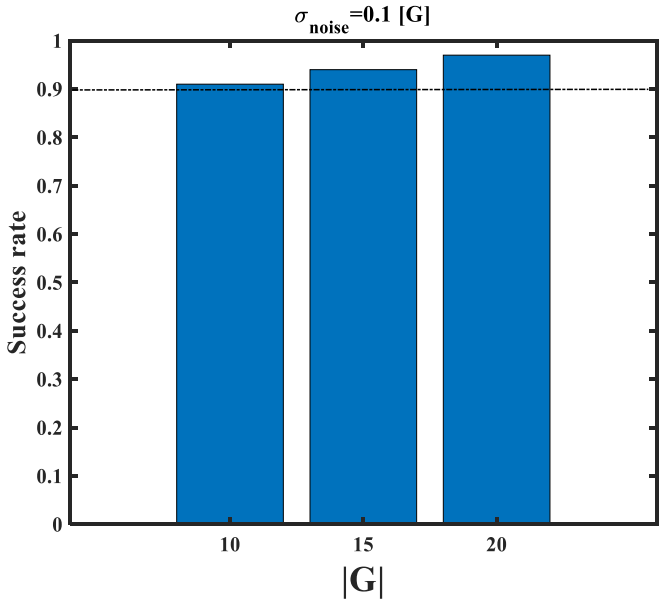


**Figure 20.** The simulated success rate of the $n = 1$ RWM control in the presence of sensor noise versus the feedback gain amplitude. Simulated with a PD controller $K_p$=1.0, $K_d$=0.5, the sensor noise has standard deviation of $\sigma_{noise} = 0.1$ G , the plasma pressure corresponds to $C_\beta = 0.73$ and the on-axis plasma rotation is $\Omega_0 = 0.05\ \Omega_A$.

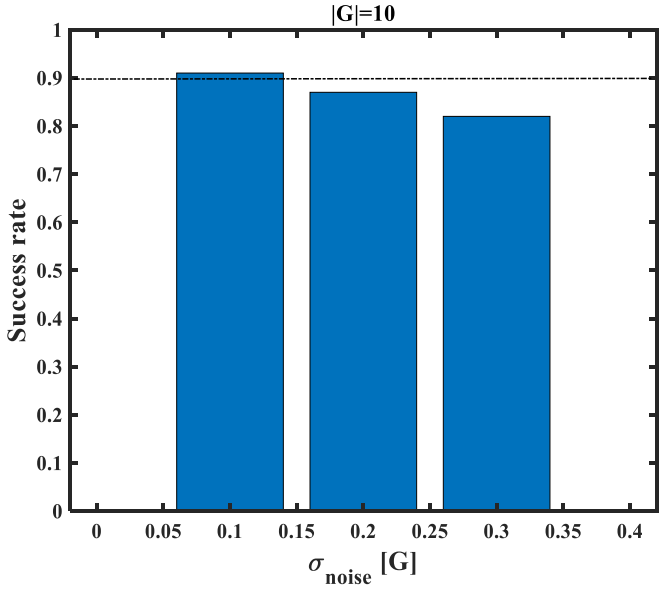


**Figure 21.** The simulated success rate of the $n = 1$ RWM control versus the sensor noise $\sigma_{noise}$. Simulated with a PD controller $K_p$=1.0, $K_d$=0.5, the feedback gain amplitude is $|G|$=10, the plasma pressure corresponds to $C_\beta = 0.73$ and the on-axis plasma rotation is $\Omega_0 = 0.05\ \Omega_A$.

location of the sensor coils $\rho_c = |R_{mag} - R_c|/a$ , $a$ is the minor radius, with $c = 0.044, a_q = -1.07$ , $a_{li} = 1.2, a_\rho = -2.9$ . These data come from fits to conventional tokamaks --- JET, ASDEX-U and COMPASS, but not spherical tokamaks. We now compare this result against MAST data. As $li(3)$ was not readily available we use $li(2) = 2V\langle B_\theta^2 \rangle / \mu_0^2 I_p^2 R_{mag}$ and unlike de Vries simply use $B_\theta = 0.2 * I_p[\mathrm{MA}]/a$ , the result is plotted in Fig. 22. So, the de Vries formula still applies but with $c = 0.044/0.58 = 0.076$ . For the studied equilibrium, $li(2) = 0.4$ , $q_{95} = 5.07, \rho_c = 1.23$ , $I_p = 21.2$ MA, $a = 1.51$ m so $B_\theta = 2.81$ T and Eq. (2) yields the disruption threshold of $B_{ML} = 70$ G . It should be noted that this is a criterion on the radial magnetic field of the locked mode. For the RWM the modes rotate relatively slowly, but are not locked. In this state the poloidal field is enhanced by the wall currents and radial field is reduced [47]. For this reason in comparisons of Eq. (2) with our modelling, we use the sensor poloidal field.

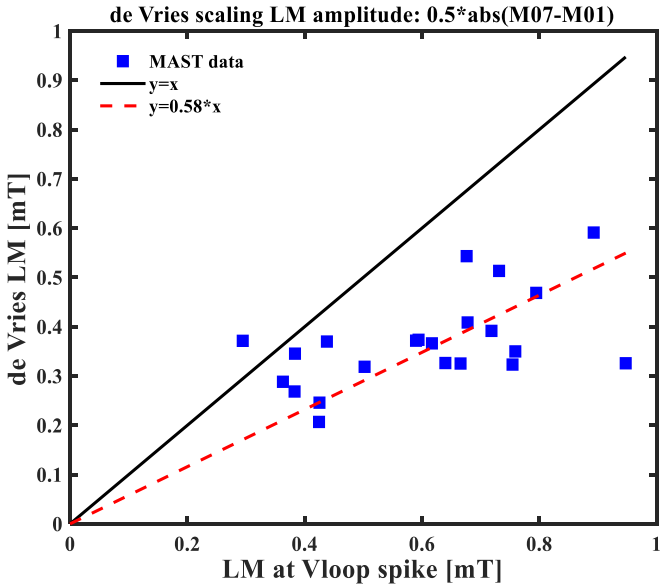


**Figure 22.** Comparison of the pre-disruption locked mode amplitude to the prediction by Eq. (2) for a range of MAST pulses.

In Fig. 23, we plot the percentage of average (Fig. 23(a), (c), (e)) and maximum (Fig. 23(b), (d), (f)) sensor amplitude over the 100 simulations for each gain between 0.1 and 1 *s*. Neither the average (the average of |Sine| is 0.5*Sine wave amplitude, so one could interpret twice the average amplitude), nor the maximum sensor amplitude, reach the

predicted disruptive amplitude of 70 G. For the $|G|$=10 case the maximum amplitude is 17.8 G, which is 25.4% of the disruptive amplitude. The success rate judged by this criterion is 100%, means the RWM will not load to a disruption with the sensor noise $\sigma_{noise} = 0.1$ G.

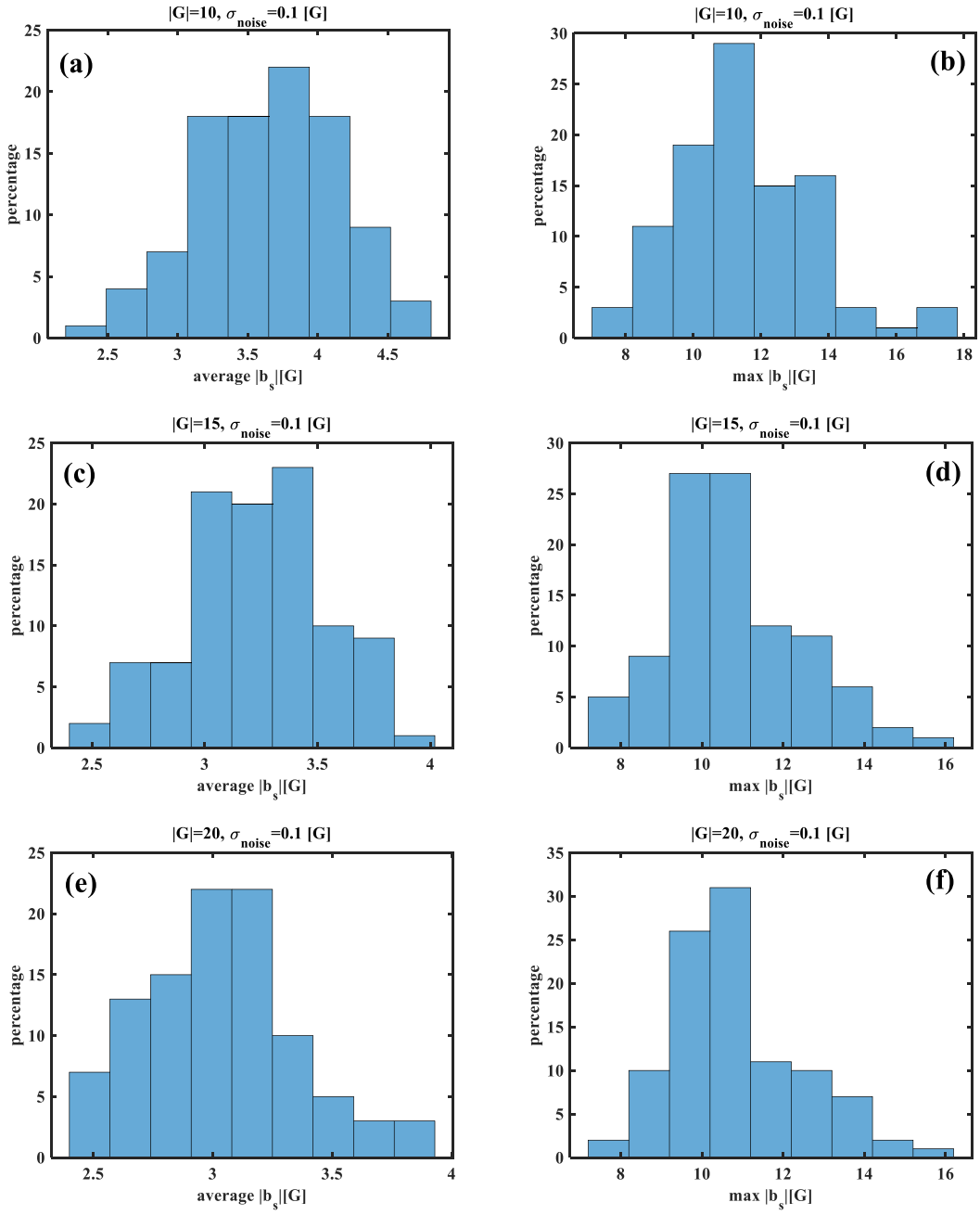


**Figure 23.** Left panels (a), (c) and (e): the percentage of average sensor amplitude over 100 simulations for each gain (the average is taken between 0.1 and 1 s to avoid initial phase when feedback is not applied). Right panels (b), (d) and (f): similar to the left panels but showing the maximum amplitude reached between 0.1 and 1 s.

## 6. Conclusion

We have carried out a comprehensive numerical investigation of the $n$ = 1 RWM stabilization for a representative spherical tokamak equilibrium using the MARS-F/K codes, taking into account (i) toroidal plasma flow and drift kinetic resonance damping from both thermal and energetic particles, (ii) the flux-to-voltage control scheme with different controller, i.e. P or PD controller, and (iii) the presence of sensor signal noise.

For typical NBI parameters and equilibrium parameters, expected for the STEP prototype, it is found that passive stabilization of the RWM yields a relatively small increase in $\beta_N$ above the no-wall limit, relying on toroidal plasma flow and drift kinetic effects. The effect of the precessional drift resonance with the NBI fast ions has a very limited effect on the growth rate of the $n$=1 RWM and the EPs contribution slightly destabilizes the RWM. In order to optimize performance from an MHD viewpoint, active control of the unstable RWM is thus desirable.

Using a set of mid-plane active coils for the RWM feedback control, it is found that with flux-to-voltage control logic, the P controller alone cannot achieve complete feedback stabilization, even combined with plasma flow and/or drift kinetic damping. Instead, by adding a modest derivative action into the controller, i.e. PD controller, and in particular if the plasma rotation ($\Omega_0 = 0.05\ \Omega_A$) is considered, the $n$=1 RWM feedback control is achieved without any noise in the closed-loop.

In the presence of the sensor signal noise with a standard deviation of $\sigma_{noise} = 0.1\ \mathrm{G}$, a statistical study finds that success rates exceeding 90% are achieved, and generally increase with the proportional feedback gain. A criterion, based on the total perturbed magnetic energy of the system, is proposed to judge the control loop success. To obtain reliable results, 100 initial value closed loop simulations are performed for the same feedback configuration, with statistics drawn in terms of the success rate for the RWM suppression. On the other hand, the required power supply of control coil (voltage and current) also increases with feedback gain and with the sensor signal noise. An alternative criterion that based on the $n$=1 locked mode amplitude to trigger a disruption is applied, and this leads to the disruption threshold of $B_{ML} = 70\ \mathrm{G}$. Neither the average, nor the maximum sensor amplitude calculated by MARS-F, reach the predicted disruptive amplitude, meaning the RWM will not load to a disruption for the modelled feedback control.

## Acknowledgments

This work has been funded by STEP, a UKAEA program to design and build a prototype fusion energy plant and a path to commercial fusion. To obtain further information on the data and models underlying this paper please contact PublicaitonsManager@ukaea.uk.

## References

[1] Wilson H R *et al* 2020 *Commercialising Fusion Energy* **2053** 8-18
[2] Hender T C *et al* 2007 *Nucl. Fusion* **47** S128-S202
[3] Chu M S *et al* 1995 *Phys. Plasmas* **2** 2236
[4] Strait E J *et al* 1995 *Phys. Rev. Lett.* **74** 2483
[5] Takeji S *et al* 2002 *Nucl. Fusion* **42** 5-13
[6] Okabayashi M *et al* 2005 *Nucl. Fusion* **45** 1715-1731
[7] Brunsell P R *et al* 2003 *Phys. Plasmas* **10** 3823
[8] Bolzonella T *et al* 2008 *Phys. Rev. Lett.* **101**
[9] Wang Z R and Guo S C 2011 *Nucl. Fusion* **51** 053004
[10] Sabbagh S A *et al* 2002 *Phys. Plasmas* **9** 2085
[11] Liu Y Q *et al* 2021 *Nucl. Fusion* **61** 116022
[12] Berkery J W *et al* 2020 *Plasma Phys. Control. Fusion* **62** 085007
[13] Sabbagh S A *et al* 2006 *Phys. Rev. Lett.* **97** 045004
[14] Chu M S and Okabayashi M 2010 *Plasma Phys. Control. Fusion* **52** 123001
[15] Troyon F *et al* 1984 *Plasma Phys. Control. Fusion* **26** 209-215
[16] Liu Y Q *et al* 2008 *Phys. Plasmas* **15** 112503
[17] Berkery J W *et al* 2010 *Phys. Plasmas* **17** 082504
[18] Wang Z R *et al* 2012 *Phys. Plasmas* **19** 072518
[19] Liu Y Q and Bondeson A 2000 *Phys. Rev. Lett.* **84** 907
[20] Okabayashi M *et al* 2001 *Phys. Plasmas* **8** 2071
[21] Fransson C M *et al* 2000 *Phys. Plasmas* **7** 4143
[22] Xia G *et al* 2014 *Plasma Phys. Control. Fusion* **56** 095009
[23] Xia G *et al* 2015 *Nucl. Fusion* **55** 093007
[24] Bondeson A and Ward D 1994 *Phys. Rev. Lett.* **72** 2709
[25] Betti R and Freidberg J P 1995 *Phys. Rev. Lett.* **74** 2949
[26] Gregoratto D *et al* 2001 *Plasma Phys. Control. Fusion* **43** 1425-1439
[27] Zheng L J *et al* 2005 *Phys. Rev. Lett.* **95** 255003
[28] Ward D J and Bondeson A 1995 *Phys. Plasmas* **2** 1570
[29] Xia G *et al* 2019 *Nucl. Fusion* **59** 126035
[30] Hu B and Betti R 2004 *Phys. Rev. Lett.* **93** 105002
[31] Reimerdes H *et al* 2007 *Phys. Rev. Lett.* **98** 055001
[32] Takechi M *et al* 2007 *Phys. Rev. Lett.* **98** 055002
[33] Guo S C *et al* 2016 *Nucl. Fusion* **56** 076006
[34] Liu Y Q *et al* 2000 *Phys. Plasmas* **7** 3681
[35] Strait E J *et al* 2004 *Phys. Plasmas* **11** 2505
[36] Liu Y Q *et al* 2004 *Nucl. Fusion* **44** 77-86
[37] Liu Y Q *et al* 2016 *Fusion Science and Technology* **70** 387-405
[38] Wang S *et al* 2019 *Nucl. Fusion* **59** 096021
[39] Hanson J M *et al* 2008 *Phys. Plasmas* **15** 080704
[40] Li L *et al* 2012 *Phys. Plasmas* **19** 012502
[41] Wang S *et al* 2018 *Fusion Science and Technology* **73** 519-532
[42] Xia G *et al* 2019 *Nucl. Fusion* **59** 016017
[43] Hirvijoki E *et al* 2014 *Comput. Phys. Commun.* **185** 1310-1321
[44] Liu Y Q *et al* 2014 *Phys. Plasmas* **21** 056105
[45] Liu Y Q *et al* 2004 *Nucl. Fusion* **44** 232-242
[46] de Vries P C *et al* 2016 *Nucl. Fusion* **56** 026007
[47] Snipes J *et al* 1988 *Nucl. Fusion* **28** 1085